Reaction–diffusion based co-synthesis of stable a-and b-cobalt hydroxide in bio-organic gels

ARTICLE *in* JOURNAL OF CRYSTAL GROWTH · JANUARY 2010

Impact Factor: 1.7 · DOI: 10.1016/j.jcrysgro.2009.11.053

Journal of Crystal Growth 312 (2010) 856–862

Contents lists available at ScienceDirect

Journal of Crystal Growth

journal homepage: www.elsevier.com/locate/jcrysgro

Reaction–diffusion based co-synthesis of stable α- and β-cobalt hydroxide in bio-organic gels

Mazen Al-Ghoul [a,c,*], Houssam El-Rassy [a], Thibaud Coradin [b], Tharwat Mokalled [a]

[a] Department of Chemistry, American University of Beirut, P.O. Box 11-0236, Riad El-Solh 1107 2020, Beirut, Lebanon
[b] UPMC Univ Paris 06, UMR 7574, Chimie de la Matière Condensée de Paris, F-75005, Paris, France
[c] Center for Advanced Mathematical Sciences, American University of Beirut, P.O. Box 11-0236, Riad El-Solh 1107 2020, Beirut, Lebanon

ARTICLE INFO

Article history:
Received 18 May 2009
Received in revised form
24 November 2009
Accepted 26 November 2009
Communicated by S. Veesler
Available online 16 December 2009

Keywords:
A1. Reaction–diffusion
A1. α-$Co(OH)_2$
A1. β-$Co(OH)_2$
A1. Ostwald ripening
A1. Phase transformation

ABSTRACT

We report the preparation, dynamics of formation and extensive characterization of a stable two-phase system of crystalline α- and β-$Co(OH)_2$. The method is based on the reaction and diffusion of hydroxide ions into a biopolymer gel (agar, gelatin) containing Co(II). The spatio-temporal dynamics leading to the formation and coexistence of two polymorphs exhibit a complicated and rich pattern whereby the system proceeds as a propagating Ostwald ripening front that continuously transforms blue/green α-$Co(OH)_2$ to crystalline β-$Co(OH)_2$. Depending on the nature of the gel, the system might further exhibit fascinating Liesegang bands. The coexisting polymorphs were characterized using XRD, FTIR, UV–vis, TGA, SEM and TEM, and EPR. The FTIR spectra reveal the intercalation of water molecules and chloride ions between the hydroxyl layers in the case of α-$Co(OH)_2$. X-ray diffraction and electronic microscopy investigations confirm the aforementioned Ostwald ripening process during the phase transformation whereby almost-amorphous α-$Co(OH)_2$ dissolves to form crystalline β-$Co(OH)_2$ 5 μm in length. The UV–vis reflectance spectra reveal that the origin of the blue/green color in the α-polymorph is due to the tetrahedrally coordinated Co(II) ions existing within the octahedral Co(II) layers. The reorganization of these tetrahedral Co(II) ions in the α-polymorph to form octahedral Co(II) in the β-polymorph is shown to take place in seconds without induction time. α-$Co(OH)_2$ was found to be mesoporous while the β-polymorph is microporous with low nitrogen adsorption capacities. Due to dipole–dipole broadening, no EPR spectrum was obtained for the β-polymorphs even at low temperature. In contrast, the obtained EPR spectrum of the α-polymorph was consistent with that of Co(II) in various materials.

1. Introduction

Cobalt hydroxide is a well-known crystalline solid exhibiting two polymorphs with hexagonal layered structures denoted as α- and β-$Co(OH)_2$[1,2]. As materials, they have attracted great interest in various fields of science and technology [3–6]. α-$Co(OH)_2$ assembles in a group of hydrotalcite-like compounds that consist of positively charged $Co(OH)_{2-x}$ layers spaced by charge balancing anions (e.g. Cl^-, NO_3^-, CO_3^{2-}, etc.) as well as water molecules. This intercalation leads to a significant increase in the inter-layer spacing, usually greater than 7 Å depending on the intercalated anionic species [7]. Accordingly, these layered double hydroxides are endowed with ion exchange property [8]. The green/blue color of this class of compounds is most probably due to the existence, in addition to the octahedral Co(II), of a considerable fraction of Co(II) that is tetrahedrally coordinated to the hydroxyl ions and interstitial anions. β-$Co(OH)_2$ shows a brucite-like structure with the cobalt ions being coordinated to hydroxide ions to form edge-shared octahedral, which thereby assemble into charge-neutral layers stacked one over the other along the *c* direction. Several crystallographic studies divulged the structure of this polymorph and revealed the lack of intercalated species between the charge-neutral layers, presenting an inter-layer spacing equal to 4.6 Å [9]. Due to this octahedral symmetry, the color of β-$Co(OH)_2$ is pink.

Homogeneous precipitation [10] and electrochemical synthesis [11] are common techniques used for the synthesis of both polymorphs. α-$Co(OH)_2$ shows thermodynamic instability and transforms quickly to the stable β-form, particularly in alkaline media [12]. Although many recent advances have been accomplished, the mechanism of this conversion is still not well understood. In addition to its metastability, synthesized α-$Co(OH)_2$ exhibits low crystallinity and a poor disordered structure [13].

* Corresponding author at: Department of Chemistry, American University of Beirut, P.O. Box 11-0236, Riad El-Solh 1107 2020, Beirut, Lebanon.
Tel.: +961 1 350000x3970; fax: +961 1 365217.
E-mail address: Mazen.Ghoul@aub.edu.lb (M. Al-Ghoul).

0022-0248/$ - see front matter © 2009 Elsevier B.V. All rights reserved.
doi:10.1016/j.jcrysgro.2009.11.053

A novel synthetic method yielding excellent crystalline α- and β-$Co(OH)_2$ has been recently reported by Liu et al. [13].

We report herein the co-synthesis of stable α- and β-$Co(OH)_2$, which are characterized using various spectroscopic and microscopic techniques. We also describe the dynamics of formation of the two polymorphs, which exhibit fascinating self-organized spatial patterns. As a matter of fact, our method is inspired by an interesting phenomenon known as Liesegang banding based on a periodic precipitation pattern obtained when soluble ions interdiffuse into a gel to react and form sparingly soluble salts [14]. The role of the gel network is not only to slow down the nucleation step, as already demonstrated in other polymer-based systems [15,16], but also to prevent sedimentation and convection. The obtained bands are often parallel to the diffusion front and separated by distinct spacings [17]. We show that the dynamics of formation of the $Co(OH)_2$ polymorphs in this type of experiments is rich and complicated. In addition, both the α- and β-phases can be easily recovered from the gel phase, allowing extensive chemical and structural characterizations. The α-phase is obtained as poorly crystalline mesoporous powder, with Co^{2+} ions in both tetrahedral and octahedral sites and no Co^{3+}. In contrast, the β-phase is obtained as crystalline micron-size particles, with all Co^{2+} in octahedral environments. The simplicity of this approach opens the route to the design of model systems for fundamental investigations of nucleation/growth processes and provides a promising method for the controlled synthesis of mixed oxide materials.

2. Experimental section

2.1. Materials

All chemicals were used as received, without further purification. Agar and gelatin were supplied by Bacto, cobalt (II) chloride hexahydrate was provided by Fluka and sodium hydroxide was purchased from Riedel-de Haën.

2.2. Preparation of cobalt hydroxide Liesegang patterns

Agar gels were achieved by dissolving agar powders (1% w/w) in various cobalt (II) chloride hexahydrate $CoCl_2 \cdot 6H_2O$ solutions. The cobalt (II) concentrations were 0.2, 0.4 or 0.6 M. In the same way, gelatin was prepared by dissolving gelatin powders (5% w/w) in $CoCl_2 \cdot 6H_2O$ solutions. The organic monomers–cobalt (II) solutions were kept at rest and for polymerization in test tubes at 18 °C. A hard faint pink gel was obtained after 24 h. After marking the solid–liquid interface on the test tube, two different sodium hydroxide solutions ($[OH^-]$=0.5 or 2 M) were added on the top of the gels without disturbing them. The diffusion of the hydroxide ions through the Co(II)-doped gels as well as the morphological evolution of the gels and the formation of the colored precipitates were followed over 3 months.

2.3. Sample characterization

The colored precipitates were collected and separated after the removal of the organic network by dissolution in hot water and filtration under vacuum. All shown results were performed on solids extracted from agar. However, similar results were obtained in the case of gelatin. The chemical structures of these products were characterized by Fourier transform infrared (FTIR) spectroscopy. A Thermo Nicolet 4700 Fourier Transform Infrared Spectrometer equipped with a Class 1 laser was used for this purpose. The KBr pellet technique was applied to perform transmission experiments in the range 4000–400 cm^{-1}. X-ray diffraction (XRD) data were recorded by a Bruker d8 discover X-Ray diffractrometer equipped with Cu-Kα radiation (λ=1.5405 Å). UV–vis diffuse reflectance experiments were performed on a JASCO V-570 UV/vis/NIR spectrophotometer. Nitrogen sorption experiments were performed at 77 K and adsorption/desorption isotherms were recorded using a Quantachrome Instruments Nova 2200e high-speed surface area and pore size analyzer after degassing the samples for 5 h at 70 °C. The specific surface area was calculated according to the BET theory while the pore size and pore volume were calculated by the BJH method based on the desorption branch of the isotherms. The thermogravimetric and differential thermal analyses (TGA/DTA) were carried out under a nitrogen atmosphere on a NETZSCH TG 209 equipment between 25 and 980 °C. Scanning electron microscopy (SEM) was performed on a Cambridge stereoscan 120 microscope using gold-coated samples. Transmission electron microscopy (TEM) was performed on particles deposited on carbon-coated grid with a Philips CM12 microscope operating at 120 kV accelerating voltage. X-band (9.4 GHz) electron paramagnetic resonance (EPR) measurements were performed at temperatures ranging from 4 to 500 K, using a home-built spectrometer based on a Bruker ER 041 bridge and a Varian TE_{102} cavity.

3. Results and discussion

3.1. Dynamics of crystal growth of the two polymorphs

The tube was left for a certain period of time and photos were taken with a digital camera. The formation of both polymorphs was widely described in a previous paper [18]. Briefly, after adding the sodium hydroxide solution on the top of the gel, a blue precipitate was spontaneously obtained due to the diffusion of hydroxyl ions within the gel pores (Fig. 1b). After a few seconds, a pink precipitate appeared at the top of the former compounds, which started moving slowly down the tube (Fig. 1c). This is attributed to a formation–dissolution of blue α-$Co(OH)_2$, which transforms into pink β-$Co(OH)_2$, and then reformation of the latter beneath the former. This propagation pattern continues until it reaches a stage where the pink polymorph stops advancing (Fig. 1e). At this point, the blue polymorph grows and invades the tube downward (Fig. 1f–i). Depending on the gel, we might later on see a Liesegang band (using gelatin) or a static continuous band (using agar). Based on the recent report by Lagzi and Ueyama [19], it can be proposed that in gelatin, a high nucleation rate leads to a large number of small crystals dispersed in the polymer matrix, favouring banding. In contrast, in agar, less nuclei are formed and crystals are grown by successive aggregation, leading to more continuous and homogeneous mineralization. The case of gelatin is shown in Fig. 2. In this case, a continuous blue band is formed before banding takes place. The sequence of snapshots (Fig. 2a–d) exhibits the formation of one band. It takes about 4 h for it to form before a new one starts appearing.

It is worth noting that both polymorphs were stable for several months and that no Liesegang band pattern was observed for the pink compound. The initial stages of the formation are similar to those in a recent and interesting study by Du et al. [20], wherein the phase conversion in the presence of a NaOH solution of hydrotalcite-like $Co(OH)_{1.6}Cl_{0.4} \cdot 4H_2O$ to β-$Co(OH)_2$ has been studied using time-resolved, *in situ* energy-dispersive X-ray diffraction (EDXRD), which allows monitoring of largely spaced Bragg reflections. This compound is in principle similar to the α-$Co(OH)_2$ obtained in our experiment as will be shown later on. Using this powerful technique, the activation energy for this

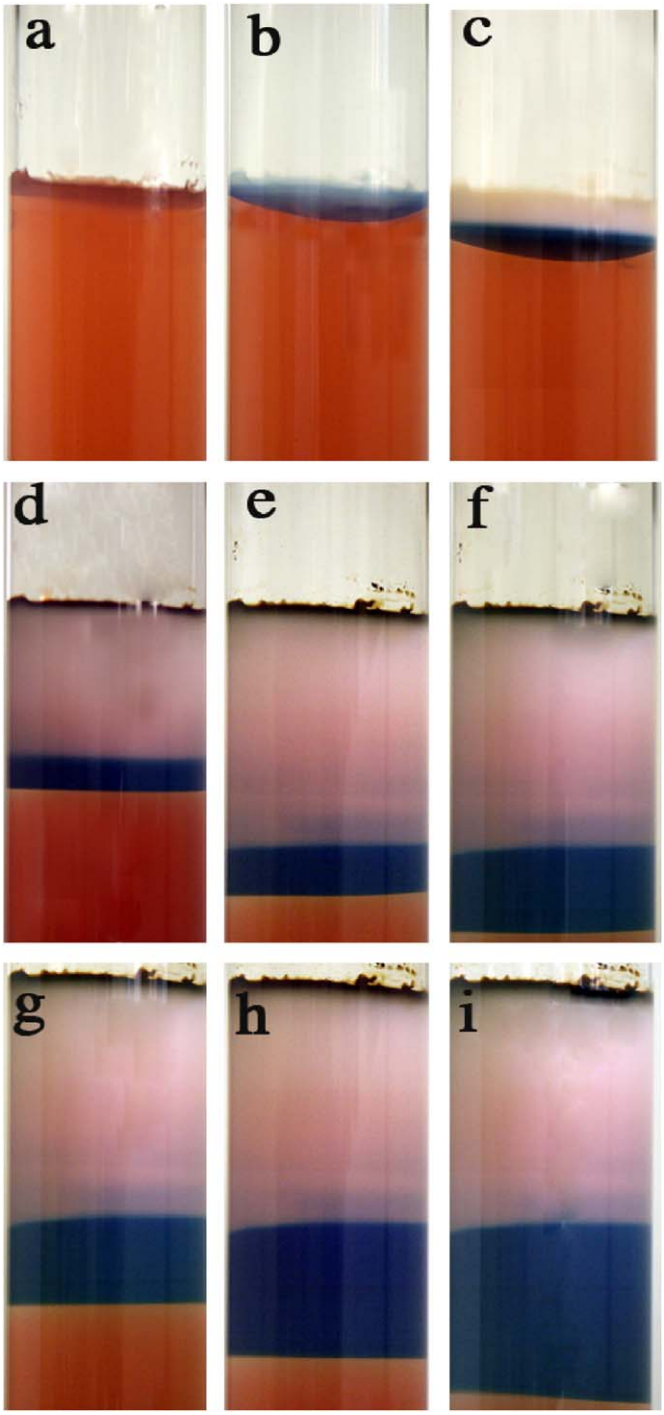

Fig.1. Formation of the stable two-phase α- and β-cobalt hydroxide. (a) Tube containing Co(II) ions in agar; (b) 1 min after addition of the hydroxide solution, a blue band of α-$Co(OH)_2$forms near the boundary; (c) 18 min after addition of the hydroxide solution, pink β-$Co(OH)_2$forms above the blue band, which propagates downward; (d) tube after 19 h: the blue front flattens and moves downward, leaving more pink behind; (e) after 40 h the pink stops advancing and the blue starts expanding; (f) after 48 h the blue band keeps expanding; (g) after 52 h; (h) after 60 h and (i) after 70 h. Notice the position of the interface between pink and blue did not change.

process, which proceeds after relatively long induction periods, was determined to be around 28.4 kJ mol^{-1}. In addition, the dependence of the rate of conversion on concentration of NaOH was determined to be proportional to $[NaOH]^{0.9}$ at 60 °C with a rate constant $k=1.78\pm0.14\times10^{3}\ s^{-1}$ and $t_{1/2}$=990 s for [NaOH]=1 M [20]. It was observed in our experiment that an increase in the NaOH concentration increases the speed of propagation of the chemical front.

Furthermore, *in situ* simultaneous small/wide-angle X-ray scattering (SAXS/WAXS) showed that the number of particles during the reaction drops to a steady state, indicative of an Ostwald ripening phenomenon [20]. This is believed to proceed through a dissolution–reformation process during diffusion, which in fact allows reconstruction of octahedrally coordinated Co(II) in the brucite-like from the tetrahedrally coordinated Co(II) in the hydrotalcite-like $Co(OH)_2$. Such dissolution–reformation gives rise to an Ostwald ripening phenomenon [21]. We will dwell on this issue further when we discuss the microscopy results.

3.2. XRD measurements

The existence of distinctive crystalline structures is revealed in the X-Ray diffractograms of the colored precipitates (Fig. 3). The patterns exhibit clearly higher crystalline nature of the pink compound than that of the blue one, as sharp *hkl* reflection peaks appeared for the former compound compared with the latter, which has relatively high signal/noise ratio. The crystallite sizes calculated from the Scherrer equation were found to be 8.4 and 13.2 nm for the α- and β-polymorph, respectively. The low crystallinity as well as the small crystallite sizes of the α-polymorph are expected to be the result of some disorder of the layers oriented along the *c*-axis, leading to a small number of parallel planes available for the diffraction; i.e. the α-polymorph is turbostratically crystallized. Coupling the chemical nature of the expected products to the positions and intensities of the diffraction peaks, we deduced with clear evidence the existence of cobalt hydroxide crystals in two distinctive structures. These hydroxides with very low solubility ($K_{sp}=1.6\times10^{-15}$) are obtained after the diffusion of the outer electrolyte (OH^-) inside the gel and its reaction with the inner electrolyte (Co^{2+}). The XRD patterns of the pink precipitate indicate undoubtedly its nature to be brucite-like β-$Co(OH)_2$ having a hexagonal cell (JCPDS card no. 30-0443). On the other hand, the blue solid is shown to be hydrotalcite α-$Co(OH)_2$ with rhombohedral symmetry. Lattice parameters of the α and β unit cells were deduced after the plane spacing calculation performed according to Bragg's equation. The α-polymorph parameters were found to be 3.15 Å (*a*) and 25.10 Å (*c*), while those of β-$Co(OH)_2$ were 3.19 Å (*a*) and 4.69 Å (*c*). It is worth emphasizing that similar results were obtained with gelatin gels, suggesting that the nature of the bio-organic network does not have a significant impact on the particle growth, at least with our reaction conditions.

3.3. FTIR spectroscopy

The FTIR spectra of both polymorphs (Fig. 4) exhibit bands centered at 3450 cm^{-1}, which are easily attributed to O–H stretching vibrations of the inter-layer water molecules and hydrogen atoms bound to OH groups. Bands appearing around 1634 cm^{-1} were assigned to the water molecules deformation vibration. The O–H stretching mode of the free Co–OH groups led to a sharp vibration peak appearing at 3631 cm^{-1}, which was more intense in β-$Co(OH)_2$ than in α-$Co(OH)_2$. This inequality is due to the existence of a greater number of free OH in the β-phase charge-neutral hydroxide layers than in the positively charged layers in the α-polymorph. In the latter polymorph, the OH vibrations are expected to be lowered because of the H-bonding between the hydrogen atoms and the intercalated anions within the layers. The broad band shown at 486 cm^{-1} corresponds to the bending vibration mode of the free Co–OH groups in the β-form. However, these vibrations are not well expressed in α-$Co(OH)_2$

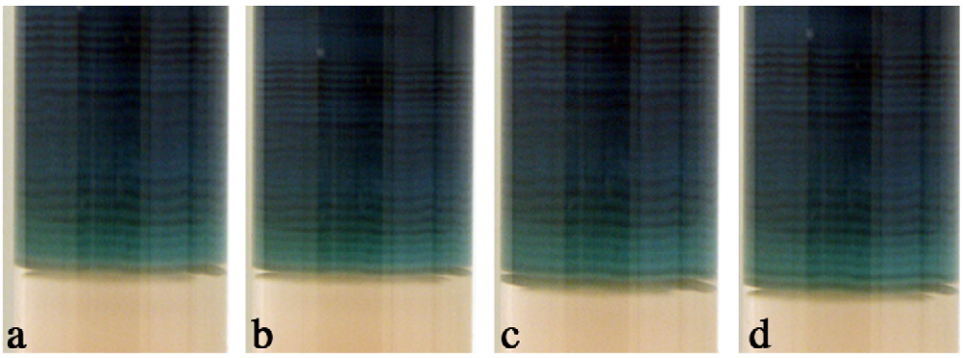

Fig. 2. Formation of Liesegang bands of α-cobalt hydroxide in gelatin. It represents a zoom-in on the banding region. (a) The last band down the tube is forming. (b) After 2 h from (a). (c) After 1 h from (b). (d) After 1 h from (c), the band in (c) is formed and a new band starts forming.

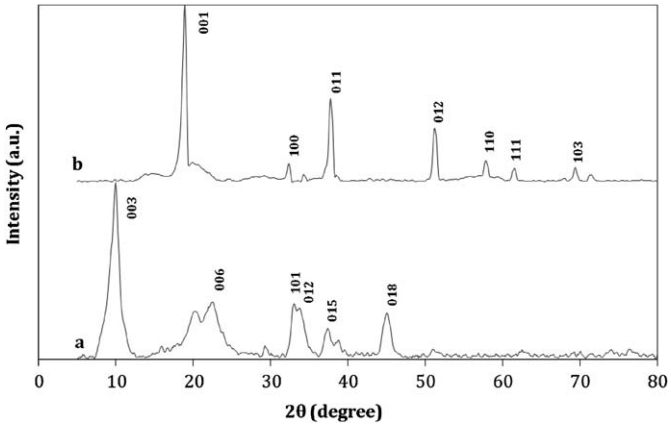

Fig. 3. Powder X-ray diffraction of (a) blue and (b) pink compounds.

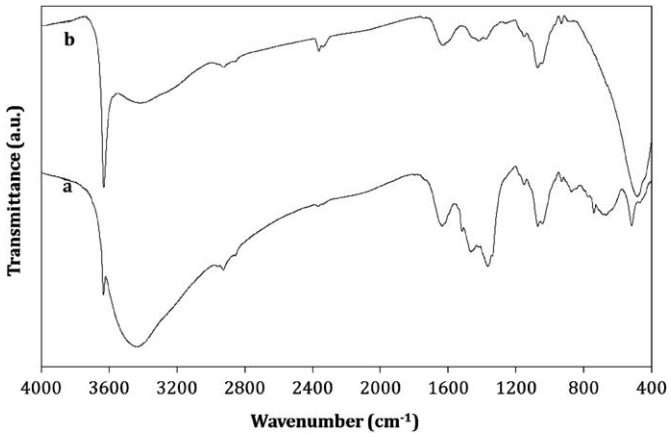

Fig. 4. FTIR spectra of (a) α-$Co(OH)_2$ and (b) β-$Co(OH)_2$.

due to constraints caused by the hydrogen bonding. The peaks around 1466 and 1072 cm^{-1} are assigned to carbonate ions present due to the dissolution of carbon dioxide molecules in water.

3.4. UV–vis diffuse reflectance

There are numerous debated theories that attempt to explain the origin of the positive charge in the α-$Co(OH)_2$ layers, which allows anions to intercalate in between these layers and endows it with a green/blue color. One theory suggests a partial substitution of the Co^{2+} by Co^{3+} ions in the octahedral layers, making the

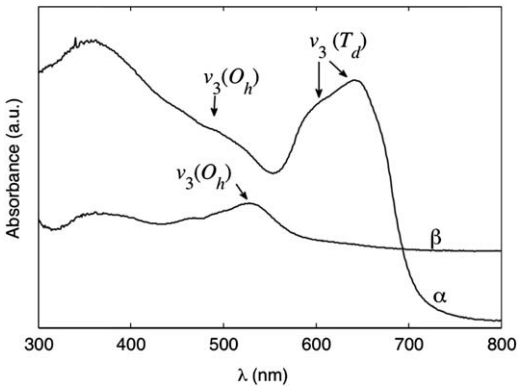

Fig. 5. UV–vis diffuse reflectance spectra of α- and β-$Co(OH)_2$. The strong bands $\nu_3(T_d)$ in α-$Co(OH)_2$ are attributed to the tetrahedral Co(II) coordination. The weak bands $\nu_3(O_h)$ in both α- and β-$Co(OH)_2$ are close to those of Co(II) in octahedral geometry.

compound analogous to layered double hydroxides (LDHs) formulated as $[Co^{2+}_{1-x}Co^{3+}_x(OH)_2]^{x+}[Cl^-_x \cdot mH_2O]$ [21,22]. Another theory suggests the existence of Co^{2+} ions that are tetrahedrally bonded to hydroxyl ions in neighboring octahedrons and to chloride anions existing between the layers [23,24].

In order to verify whether Co^{3+} is present or not in α-$Co(OH)_2$, we added $Fe(NH_4)_2(SO_4)_2 \cdot 6H_2O$ in the presence of 3 M H_2SO_4 and then titrated the mixture with a solution of standardized $KMnO_4$. The titration revealed that no Co^{3+} was present in the prepared α-$Co(OH)_2$.

UV–vis diffuse reflectance measurements were then performed on the two solid polymorphs as shown in Fig. 5. The weak bands in the visible region at ~488 and ~530 nm were observed in the spectra of both α- and β-cobalt hydroxide, respectively. Such transitions are close to the weak d–d absorption transitions observed in octahedral Co(II) complexes ($\nu_3(O_h)$=493.2 nm) [25,26]. The mere presence of such bands for β-cobalt hydroxide confirms the octahedral arrangement of Co(II), leading to the pink brucite crystals. Furthermore, strong peaks were observed at ~605 and 642 nm only for α-cobalt hydroxide. These peaks are very close to those reported for tetrahedral Co(II) complexes ($\nu_3(T_d)$=592.3 and 641.2 nm) [27]. Such strong peaks at the aforementioned wavelengths are responsible for the green/blue color of the prepared α-cobalt hydroxide.

3.5. TGA–DTA

Fig. 6 shows the TGA–DTA curves of the α- and β-cobalt hydroxide samples in the temperature range 25–980 °C, revealing distinctly different profiles with total weight losses of 41% for the

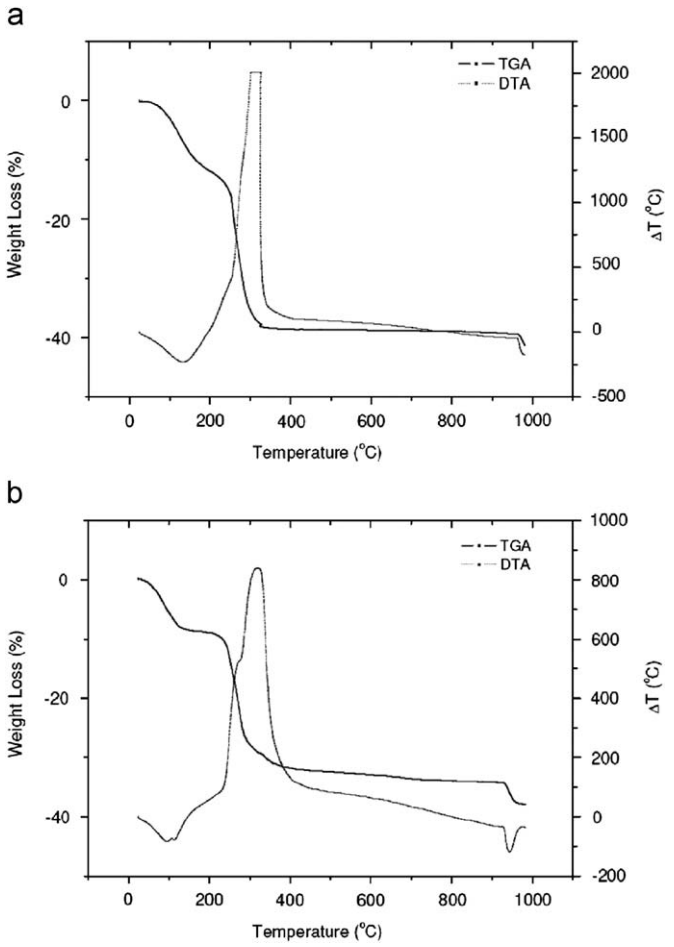

Fig. 6. Thermogravimetric and differential thermal analyses (TGA – DTA) of (a) α- and (b) β-$Co(OH)_2$.

α-polymorph and 38% for the β-phase. The weight loss of α-$Co(OH)_2$ is divided into three successive zones: the first endothermic loss below 190 °C and centered at 134 °C corresponds to 11.5% of the initial mass and is assigned to dehydration of the sample by removal of adsorbed and intercalated water molecules. The second weight loss taking place between 190 and 400 °C and centered at 325 °C is shown to be exothermic. This 27.1% weight loss corresponds to the loss of water molecules obtained after dehydroxylation of the cobalt hydroxide layers. The small decrease after 400 °C can be attributed to the loss of the chloride ions [13]. The TG curve of β-$Co(OH)_2$ shows 8.3% endothermic losses of adsorbed water centered at 94 and 112 °C according to the DTA curve [28]. An exothermic loss (23.8%) was observed between 140 and 440 °C showing two successive maxima at 272 and 319 °C, which correspond to decomposition of cobalt hydroxide into cobalt oxide. The weight loss after 440 °C can be attributed to the decomposition of CoO to form the spinel oxide Co_3O_4[28].

3.6. Scanning and transmission electron microscopy

The microstructure of both polymorphs was investigated by scanning electron microscopy after coating the samples with a thin gold film (Fig. 7). The SEM images reveal the existence of a dense and compact phase, which confirms the low crystallinity of α-$Co(OH)_2$; no crystals were observed even at high magnification ($\times$10,000). However, SEM micrographs of the β-polymorph divulge the existence of crystals approximately 5 μm in length,

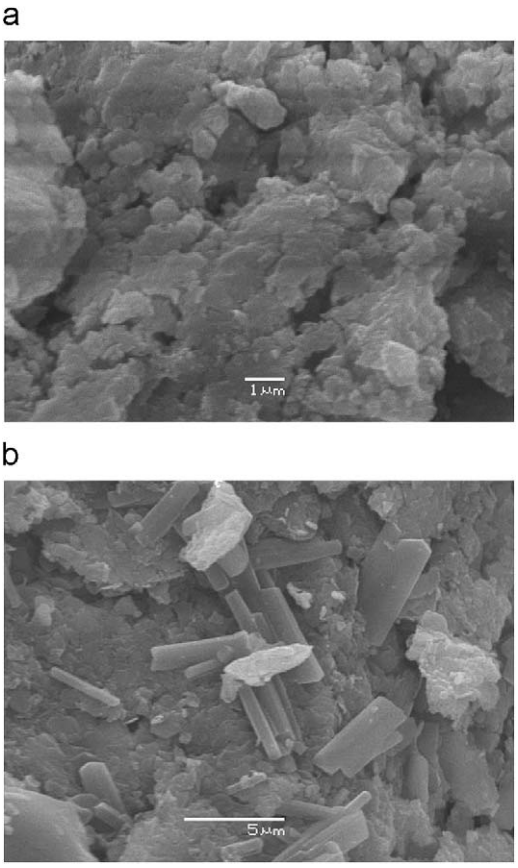

Fig. 7. Scanning electron microscopy images of (a) α- and (b) β-$Co(OH)_2$.

together with plate-like crystals. The abundance of the crystals in this sample could be easily correlated to the intense diffraction peaks obtained for the same material by XRD.

The TEM micrographs of the prepared α- and β-cobalt hydroxide are shown in Fig. 8. The α-phase images show an amorphous material with no crystalline structure. It is worth noting that neither crystals nor crystalline planes were observed although the XRD spectrum for this material (Fig. 3) shows broad peaks. On the other hand, the β-$Co(OH)_2$ images revealed the existence of hexagonal crystals easily identified. Electron diffraction on these crystals disclosed the crystalline structure of this material and at very high magnification; the hexagonal crystals exhibit a perfectly ordered structure, where the measured inter-layer spacing was 4.8 Å (Fig. 9). This interplanar spacing is in excellent agreement with the results found in XRD. Such a behavior confirms the fact that Ostwald ripening is taking place, whereby crystalline β-$Co(OH)_2$ is formed at the expense of the smaller almost amorphous α-$Co(OH)_2$ existing in the gel. What is interesting here is that, contrary to the finding of Du et al. [20], where the phase transformation reaction is preceded by relatively long induction times (for example 419 s for [NaOH]=2 M and at a temperature of 60 °C), the transformation reported here took place after a couple of minutes as shown in Fig. 1b. This means that the reconstruction of octahedral Co(II) in the layers from the tetrahedral ones existing in turbostratically disordered α-$Co(OH)_2$, which in fact involves the breaking and forming of bonds, proceeds at relatively faster rates by a dissolution–reformation process.

3.7. Nitrogen adsorption isotherms

The nitrogen adsorption in Fig. 10 performed for both solid materials revealed different porous natures of the two polymorphs. The isotherms performed on the α-phase revealed

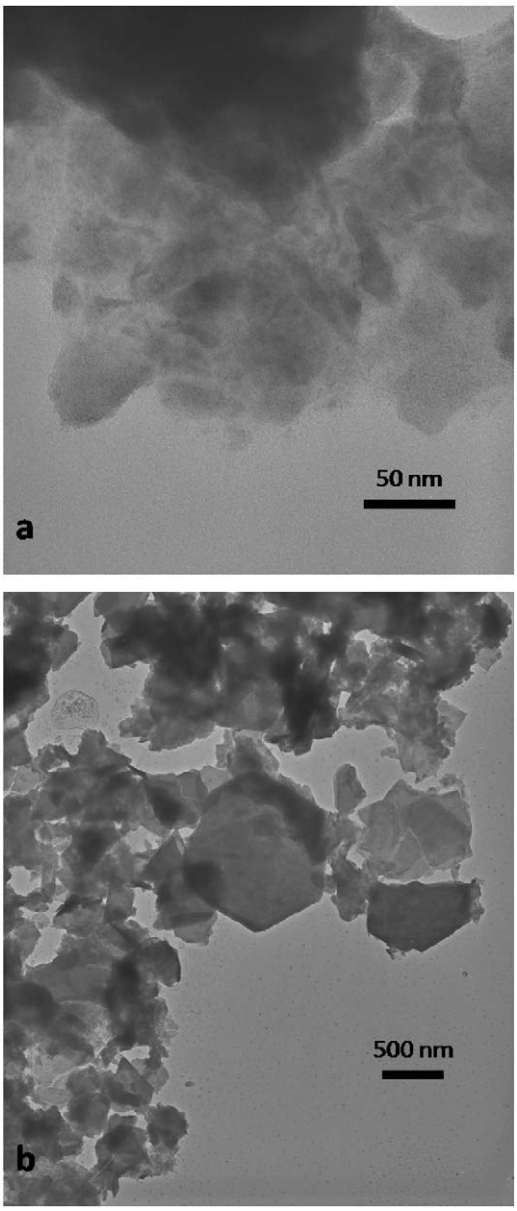

Fig. 8. Transmission electron microscopy images of (a) α- and (b) β-$Co(OH)_2$.

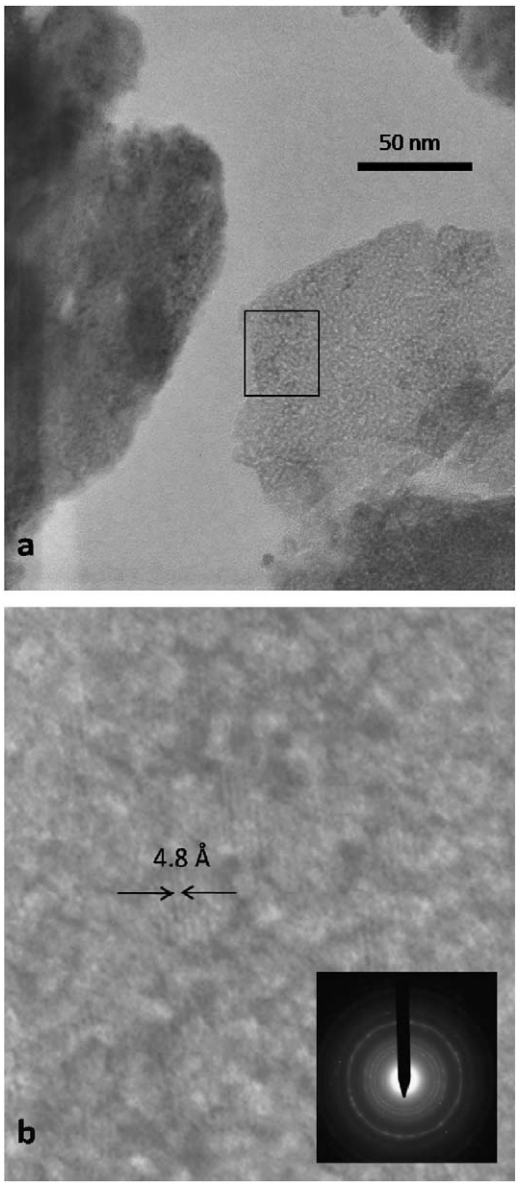

Fig. 9. TEM micrographs of (a) β-$Co(OH)_2$ at 340 K magnification and (b) β-$Co(OH)_2$ at high magnification showing the crystal planes and the electron diffraction pattern.

a mesoporous nature of these materials, where the specific surface area calculated according to the BET theory was found to be 26 $m^2\,g^{-1}$, the pore volume equal to 0.26 $cm^3\,g^{-1}$ and the pore size distribution centered at ca. 17 nm. However, the β-$Co(OH)_2$ isotherms displayed a very weak nitrogen adsorption; its specific surface area was calculated to be ca. 5 $m^2\,g^{-1}$ and the pore volume ca. 0.012 $cm^3\,g^{-1}$. As the porous structure is expected to arise from interparticle porosity, such a difference between the α and β-phases reflects the very dense structure of the latter compared to the former, which is in excellent agreement with what was observed in electron microscopy.

3.8. Electron paramagnetic resonance (EPR)

EPR measurements were performed at liquid nitrogen temperature using a Varian X-band EPR spectrometer equipped with an Oxford Instrument helium gas flow cryostat. The nitrogen flow was injected onto the sample and the temperature was measured using a thermocouple. No room temperature EPR signal was observed for both samples α-$Co(OH)_2$ and β-$Co(OH)_2$. However, as the temperature was decreased below 200 K, a weak and broad signal was observed in α-$Co(OH)_2$. The line intensity increased further as the temperature lowered to 110 K and the signal linewidth was about 40 mT. The large linewidth of the signal is probably due to dipole–dipole broadening [29,30], while experiments performed in the range of temperature 110–300 K did not show any signal for β-$Co(OH)_2$. The spectrum of α-$Co(OH)_2$ is shown in Fig. 11. Analysis of the line position lead to an average Landé factor $g=2.21\pm0.02$, which is consistent with values reported in the literature for Co^{2+} in various host materials [30,31].

4. Conclusion

We report a stable two-phase system consisting of α- and β-$Co(OH)_2$ using reaction–diffusion of Co(II) and hydroxide ions in bio-organic gels. The system is shown to proceed through a

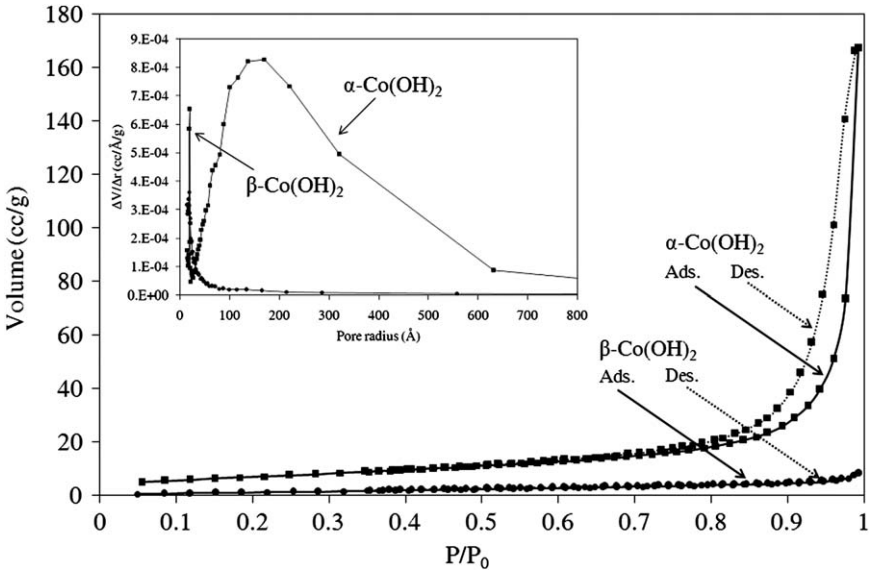

Fig. 10. α- and β-$Co(OH)_2$ nitrogen adsorption–desorption isotherms and their corresponding pore size distribution (inset).

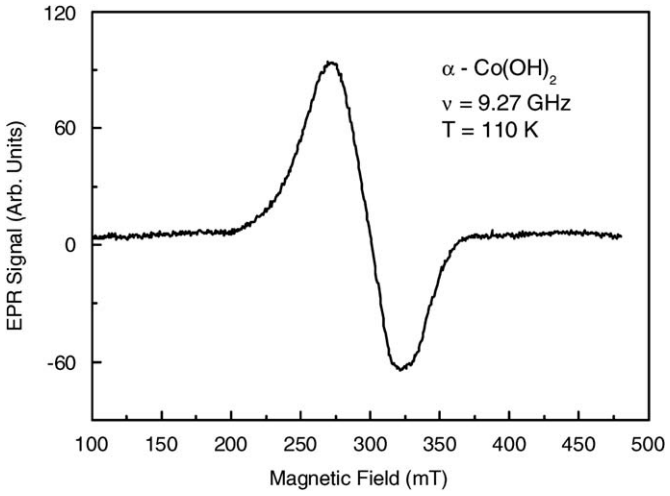

Fig. 11. X-band (9.27 GHz) powder EPR spectrum for α-$Co(OH)_2$.

continuous Ostwald ripening process that transforms one polymorph to the other, giving rise to an interesting propagating chemical front. The Ostwald ripening mechanism was confirmed using various microscopy techniques. The method sheds some light on the not very well understood phase conversion of the different polymorphs of cobalt hydroxide. It will also help in understanding Ostwald ripening in these types of systems and how one can tailor the system to target certain crystal sizes and shapes. The dynamics of formation of the two phases is also worth investigating theoretically from the point of view of reaction–diffusion coupled to nucleation, growth and competitive particle size formulation. Experimentally, this method opens the door to a wide range of precipitate systems as well as the study of the effect of some important parameters such as the gel pore size, temperature, electric field and the nature of the intercalating anion (e.g. substituting cobalt (II) chloride with cobalt (II) sulfate, citrate, nitrate, bromide, etc.). This method is currently applied to synthesize nano-sized ferrite and cobalt ferrite materials.

Acknowledgements

The authors gratefully acknowledge the funding provided by the American University of Beirut Research Board. They are also thankful to Dr. Samih Isber for his help in the EPR measurements and Dr. Tarek Ghaddar for very helpful discussions.

References

[1] D.L. Bish, A. Livingstore, Mineral. Mag. 44 (1981) 339.
[2] P. Oliva, J. Leonardi, J.F. Laurent, C. Delmas, J.J. Braconnier, M. Figlarz, F. Fievet, A. Guibert, J. Power Sources 8 (1982) 229.
[3] L. Cao, F. Xu, Y.Y. Liang, H.L. Li, Adv. Mater. 16 (2004) 1853.
[4] P. Elumalai, H.N. Vasan, N. Munichandraiah, J. Power Sources 93 (2001) 201.
[5] A. Rujiwatra, C.J. Kepert, J.B. Claridge, M.J. Rosseinsky, H. Kumagai, M. Kurmoo, J. Am. Chem. Soc. 123 (2001) 10584.
[6] H. Itahara, C. Xia, J. Sugiyama, T. Tani, J. Mater. Chem. 14 (2004) 61.
[7] Y. Zhu, H. Li, Y. Koltypin, A. Gedanken, J. Mater. Chem. 12 (2002) 729.
[8] A. Ookubo, K. Ooi, H. Hayashi, Langmuir 9 (1993) 1418.
[9] P. Benson, G.W.D. Briggs, W.F.K. Wynne-Jones, Electrochim. Acta 9 (1964) 275.
[10] M. Dixit, G.N. Subbanna, P.V.ishnu Kamath, J. Mater. Chem. 6 (1996) 1429.
[11] R.S. Jayashree, P.V. Kamath, J. Mater. Chem. 9 (1999) 961.
[12] A. Gaunand, W.L. Lim, Powder Technol. 128 (2002) 332.
[13] Z. Liu, R. Ma, M. Osada, K. Takada, T. Sasaki, J. Am. Chem. Soc. 127 (2005) 13869–13874.
[14] R.E. Liesegang, Naturwiss. Worchenschr 11 (1896) 353.
[15] J. Zhang, S. Xu, E. Kumacheva, J. Am. Chem. Soc. 126 (2004) 7908.
[16] R. Brayner, M.-J. Vaulay, F. Fiévet, T. Coradin, Chem. Mater. 19 (2007) 1190.
[17] S.C. Muller, J. Ross, J. Phys. Chem. A 107 (2003) 7997.
[18] H. El-Batlouni, H. El-Rassy, M. Al-Ghoul, J. Phys. Chem. A 112 (2008) 7755.
[19] I. Lagzi, D. Ueyama, Chem. Phys. Lett. 468 (2009) 188.
[20] Y. Du, M. Ok, D. O'HareJ. Mater. Chem. 18 (2008) 4450.
[21] S. Ostwald, Z. Phys. Chem. 22 (1897) 289.
[22] W.T. Reichle, Solid State Ion. 22 (1986) 135.
[23] P.V. Kamath, G.H.A. Therese, J. Gopalakrishnan, J. Solid State Chem. 128 (1997) 38.
[24] R. Ma, Z. Liu, K. Takada, K. Fukuda, Y. Ebina, Y. Bando, T. Sasaki, Inorg. Chem. 45 (2006) 3964.
[25] L. Poul, N. Jouini, F. Fievet, Chem. Mater. 12 (2000) 3123.
[26] A.B.P. Lever, in: Inorganic Electronic Spectroscopy, Elsevier, New York, 1984.
[27] W. Stahlin, H.R. Oswald, Acta Crystallogr. B 26 (1970) 860.
[28] C. Duval, in: Inorganic Thermogravimetric Analysis, 2nd edition, Elsevier Publishing Company, 1963.
[29] B. Cage, P. Cevc, R. Blinc, L.C. Brunel, N.S. Dalal, J. Magn. Reson. 135 (1998) 178.
[30] A. Abragam, B. Bleaney, in: Electron Paramagnetic Resonance of Transitions Metal Ions, Oxford University Press, New York, 1970.
[31] S. Isber, M. Averous, Y. Shapira, V. Bindilatti, A.N. Anisimov, N.F. Olivera, V.M. Orera, M. Demianiuk, Phys. Rev. B 51 (1995) 15211.